NJC

ROYAL SOCIETY OF CHEMISTRY

PAPER

View Article Online
View Journal

Cite this: DOI: 10.1039/d5nj03028e

Linkage isomerism in a homoleptic Fe(II) complex with BODIPY-1*H*-tetrazole ligands

Matthias Schöbinger, †*[a] Martin Huber, †[a] Berthold Stöger [b] and Peter Weinberger [a]

Received 25th July 2025,
Accepted 7th January 2026

DOI: 10.1039/d5nj03028e

rsc.li/njc

We examined the coordination behavior of the sterically demanding 4,4-difluoro-1,3,5,7-tetramethyl-8-[(1*H*-tetrazol-1-yl)methyl]-4-bora-3a,4a-diaza-*s*-indacene ligand **L** in octahedral Fe(II) coordination compounds. Using four different solvents – $ClCH_2CN$, $BrCH_2CN$, CH_3OH, and $(CH_3)_2CO$ – five unique crystal structures were obtained and characterized by single-crystal X-ray diffraction. In $ClCH_2CN$ and $BrCH_2CN$, **L** coordinated equatorially through N4 and apically through its less basic N3 atom, yielding a pseudo-homoleptic $[Fe(\mathbf{L}^{N4})_4(\mathbf{L}^{N3})_2]^{2+}$ architecture. This represents the first documented example of monodentate 1*H*-tetrazole N3/N4 linkage isomerism in an Fe(II) complex. Conversely, O-donor solvents (CH_3OH and $(CH_3)_2CO$) resulted in the formation of a heteroleptic $[Fe(\mathbf{L})_4(solvent)_2]^{2+}$ motif, in which the solvent molecules coordinated through their O-atoms and occupied two coordination sites. The CH_3OH adduct underwent a topotactic single-crystal-to-single-crystal transformation upon air exposure, exchanging CH_3OH for H_2O, and was stabilized by extensive hydrogen bonding. Unlike classical $[Fe(1\text{-alkyl-}1H\text{-tetrazole})_6]^{2+}$ systems, none of the investigated coordination compounds exhibited SCO properties, instead remained locked in a single spin state. These findings demonstrate that steric bulk can override the ligand's N4 coordination preference to Fe(II), either by enforcing N3 coordination or by permitting coordination of co-ligands, and thus provide guidance for the design of 1*H*-tetrazole-based Fe(II) materials.

Introduction

Tetrazoles (tz), five-membered heterocycles containing four adjacent nitrogen atoms, have attracted considerable attention across coordination chemistry, materials science, and medicinal chemistry. Their unique properties including stability, acidity and basicity, high dipole moment, high formation enthalpy among others make them ideal building blocks for functional materials and bioactive molecules.[1–5]

Tz exists in two stable tautomeric forms (1*H*-tz and 2*H*-tz), each of which can be mono- or disubstituted (Scheme 1). Monosubstitution occurs at N1, N2, or C5, whereas disubstitution yields 1,5-; 2,5- or 5,5-derivatives.[6] The four donor nitrogen atoms of tz enable a wide variety of coordination modes to transition metals, which strongly depend on the substitution pattern.[7] Since the pioneering work of Franke *et al.* in 1982, who first reported an octahedral Fe(II) complex of *N*1-alkyltetrazoles exhibiting spin crossover (SCO) behavior,[8] this ligand class has attracted growing interest for Fe(II) SCO materials, owing to their optimal ligand field strength.[9] Within the *N*1-substituted tetrazole ligands, the N4 nitrogen is the most

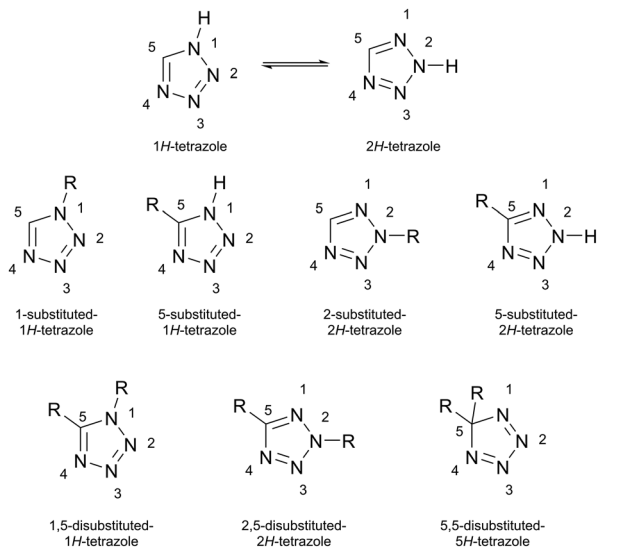

Scheme 1 Tautomeric forms of tetrazole and their mono- and disubstituted derivatives.

[a] *Institute of Applied Synthetic Chemistry, TU Wien, Getreidemarkt 9/163, 1060, Vienna, Austria. E-mail: matthias.schoebinger@tuwien.ac.at, peter.e163.weinberger@tuwien.ac.at*
[b] *X-Ray Center, TU Wien, Getreidemarkt 9/164, 1060, Vienna, Austria*
† These authors contributed equally.

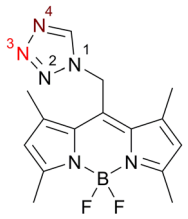

L

Chart 1 Chemical structure of **L** with highlighted coordinating atom(s) for **1** and **2**: N4 (dark red) and N3 (light red), for **3** and **4**: N4 (dark red).

basic site, followed by N3.[10] Consequently, *N*1-substituted tetrazoles coordinate exclusively in a monodentate fashion through the N4 donor atom to Fe(II).[9] In contrast, C5-substituted tetrazoles exhibit a broader range of binding motifs, including bridging interactions between Fe(II) centers.[3,11–14]

To realize extended SCO coordination polymers from N1-substituted tetrazoles 1,ω-di(tetrazol-1-yl) derivatives have been employed to bridge Fe(II) centers, yielding 1D,[15–17] 2D,[18] and 3D frameworks.[19,20]

Using N1-substituted tetrazoles as ligands with Fe(II) salts of non-coordinating anions (**A**; *e.g.*, BF_4^-, ClO_4^-) typically yields homoleptic, mononuclear complexes of the general formula $[Fe(R\text{-tetrazol-1-yl})_6]\mathbf{A}_2$, in which six N1-substituted tetrazole ligands occupy an octahedral coordination sphere.[21–26] Heteroleptic analogues are still relatively rare. Mononuclear examples featuring axial coordination by water[27] or anions such as NCS^-[28] have been reported; however, axial coordination of organic nitrile co-ligands has so far been restricted to polymeric networks in which bridging 1,ω-di(tetrazol-1-yl)alkane ligands occupy the equatorial positions.[29–31]

In our previous work, we described the first heteroleptic mononuclear Fe(II) complex bearing organic nitriles (RCN; R = alkyl, alkenyl, aryl) co-ligands, $[Fe(\mathbf{L})_4(RCN)_2]\mathbf{A}_2\cdot x\mathbf{solv}.$,[32,33] where **L** is the tetrazol-1-yl ligand functionalized with a BODIPY (4,4-difluoro-1,3,5,7-tetramethyl-4-bora-3a,4a-diaza-*s*-indacene) fluorophore in N1 position of tz (Chart 1),[34] **A** the non-coordinating anion and **solv**. the crystal solvates. Some coordination compounds of this family undergo a thermally induced spin transition from a low-spin (LS, $S = 0$) to a high-spin (HS, $S = 2$) state with a modest synergistic response of its photoluminescence signal. To enhance the modulation of the PL signal and probe its influence on the spin crossover (SCO) behavior, we now target a homoleptic analogue $[Fe(\mathbf{L})_6](ClO_4)_2$ featuring six **L** ligands coordinated to Fe(II).

Although strategies to selectively control the formation of heteroleptic *versus* homoleptic complexes have not been explored, we propose that judicious solvent selection during complexation can steer the system toward a homoleptic architecture, thereby tuning both SCO behavior and photoluminescence response.

Results and discussion

Synthesis

The synthesis of the ligand **L** and the coordination compounds **1–4** was carried out according to previously described procedures.[32–34] **L** and $Fe(ClO_4)_2\cdot 6H_2O$ were mixed and stirred in different solvents ($ClCH_2CN$ (**1**), $BrCH_2CN$ (**2**), acetone (**3**) and CH_3OH (**4a**)) at 40 °C overnight. The crude products were precipitated and washed with diethyl ether (Et_2O) to yield **1–4a** in moderate yields (Schemes 2 and 3).

In contrast to our recent studies,[32,33] where the use of nitrile solvents (RCN) led to the formation of heteroleptic complexes with RCN as co-ligands, a homoleptic coordination environment was obtained in **1**. This coordination mode was reproducible with the related nitrile $BrCH_2CN$ in **2**, but not when weaker coordinating solvents such as acetone or methanol were used, as in **3** and **4**.

Reaction monitoring was performed using X-ray powder diffraction (XRPD) and IR spectroscopy, with the $\nu_{CH(tz)}$ band serving as an indicator of successful complexation.

Remarkably, coordination compound **4b** was obtained from **4a** in a single-crystal-to-single-crystal (SC-to-SC) transformation (*vide infra*, Scheme 3).

Crystal structures

Single crystals (SCs) of coordination compounds **1–4** were obtained *via* slow diffusion of Et_2O into saturated solutions of the respective solvents – $ClCH_2CN$ for **1**, $BrCH_2CN$ for **2**, acetone for **3**, and CH_3OH for **4** – at room temperature (rt).

Coordination compound **1** crystallizes in the triclinic $P\bar{1}$ space group and features one crystallographically unique mononuclear complex located on a center of inversion. The complex exhibits a homoleptic octahedral coordination environment, consisting of six molecules of **L**. However, contrary to our expectations only four molecules of **L** coordinate *via* their tetrazolic *N*4-atom (the italicized numbered N-atoms correspond to the tetrazole numbering system in Chart 1), whereas two molecules of **L** coordinate *via* their tetrazolic *N*3-atom (Fig. 1 and Fig. S3). This *N*3-coordination mode of a monodentate *N*1-substituted tetrazole remains hitherto unknown since, in Fe(II) coordination compounds, these ligands coordinate preferably *via* their *N*4-atom.[9] Coordination through the *N*3-atom is shown in literature typically only in a bidentate binding mode of *N*1-substituted tz with *e.g.* coinage metals. In the case of **L** such a bidentate coordination mode was previously shown in Ag coordination compounds by our group.[35] To our knowledge, this is the first report of a tetrazole N3/N4 linkage isomerism[36] in a Fe(II) system bearing monodentate tetrazol-1-yl

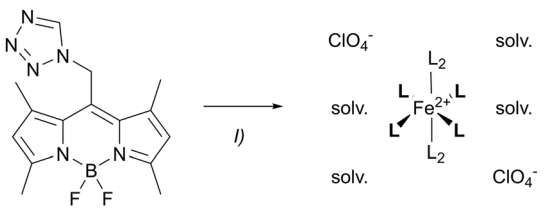

1, L_2...**L** (*N3*); solv....$ClCH_2CN$
2, L_2...**L** (*N3*); solv....$BrCH_2CN$
3, L_2...$(CH_3)_2C$=O; solv....non

Scheme 2 Synthesis of coordination compounds **1–3**, reagents and conditions: (I) $Fe(ClO_4)_2\cdot 6H_2O$, $ClCH_2CN$ (**1**), $BrCH_2CN$ (**2**), acetone (**3**) 40 °C, o.n., 75.3% (**1**), 68.9% (**2**), 56.6% (**3**).

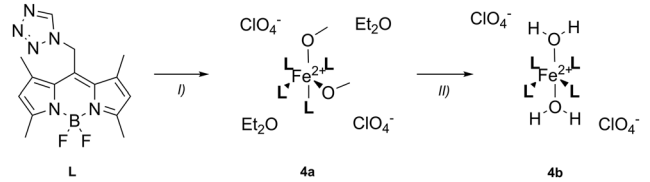

Scheme 3 Synthesis of coordination compounds **4a** and **4b**, reagents and conditions: (I) $Fe(ClO_4)_2{\cdot}6H_2O$, CH_3OH, 40 °C, o.n., 41.7% (**4a**); (II) **4b** was obtained from **4a** *via* a SC-to-SC transformation under ambient conditions (air humidity), occurring essentially instantaneously.

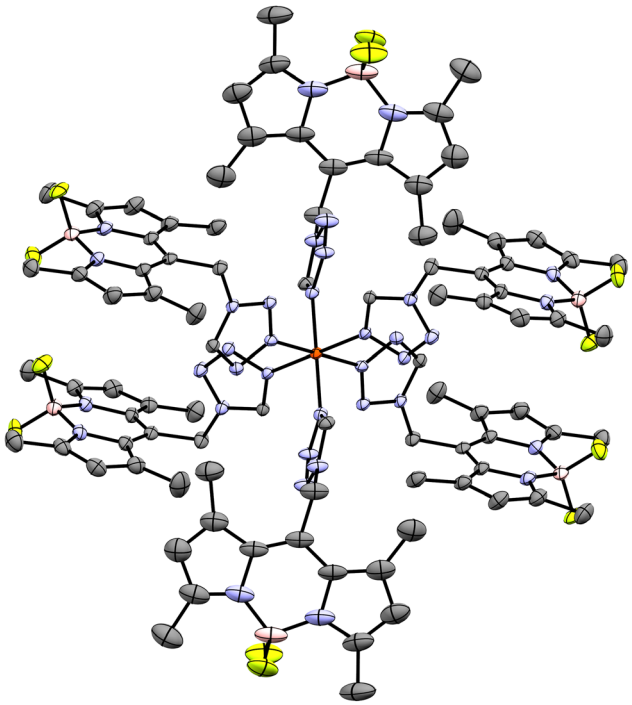

Fig. 1 Molecular structure of the homoleptic mononuclear complex of coordination compound **1** at 100 K, exhibiting linkage isomerism of **L**; *N*3 coordination mode of **L** in the equatorial plane front right and back left (ellipsoids: 50% probability level; atom color code: pink…B, grey…C, blue…N, light green…F, orange…Fe; solvate molecules, non-coordinating anions and H-atoms are omitted for clarity).

ligands. Note that the N and C-Atoms of the tz rings could be unambiguously assigned owing to their different atomic form factors and the H-atom attached to C was in all cases clearly located in the difference Fourier map. The **L** molecules in the *trans* arrangement are crystallographically equivalent, whereas those in *cis* position are conformers (Fig. S1 and S2). These conformers differ in the orientation of the tz moiety relative to the FBF plane of the BODIPY core, as previously established by structural and theoretical studies on **L**.[34]

Each mononuclear complex is accompanied by two non-coordinating anion molecules (ClO_4^-) and four intercalated solvent molecules ($ClCH_2CN$) (Fig. S4). These solvent molecules are disordered about two positions with an occupancy ratio of 57.6 : 42.4(4) at 100 K and 53.5 : 46.5(11) at 300 K. The model derived from the 100 K measurement additionally features a diffuse electron density peak, which we interpret as water of crystallization. At 300 K the anion likewise becomes disordered about two positions with an occupancy ratio of 78.5 : 21.5(8), which can be interconverted by rotation along the Cl1–O2 axis (Fig. S6). At both measuring temperatures (100 K and 300 K) N–Fe distances (Table 1) suggest that the compound is in LS state.[37]

Coordination compound **2** is isostructural to **1** at 100 K (Fig. 2 and Fig. S7-S9). However, besides the different nitrile solvent ($ClCH_2CN$ in **1**, *vs.* $BrCH_2CN$ in **2**), **2** features no water of crystallization and the occupancy ratio of the disordered nitrile solvent molecules is different: 67.5 : 32.5(3).

Coordination compound **3** (Fig. S10–S13) crystallizes in the monoclinic $P2_1/c$ space group and features acetone as co-ligand in the apical positions, which coordinates to the Fe(II) center *via* its O-atom (Table 1 and Fig. 3). In the equatorial plane, four molecules of **L** coordinate to the Fe(II) center *via* the tetrazolic *N*4-atom. Based on the symmetry of **3**, like in **1**, the **L** molecules in the *trans* arrangement are crystallographically equivalent, whereas those in *cis* position are conformers. However, no solvent molecules are incorporated into the crystal lattice. Based on the N–Fe bond lengths (Table 1), **3** is fully in the HS state at 100 K, according to literature,[22,37–39] as expected from its coordination environment. Compared to the heteroleptic analogue $[Fe(\mathbf{L})_4(CH_3CN)_2](ClO_4)_2{\cdot}2CH_3CN$, which undergoes a thermal spin transition at $T_{1/2}$ = 265 K,[32] **3** is expected to exhibit

Table 1 Structural parameters for coordination compounds **1–4**

Compound	*T*/K	Spin state	N12(tz)-Fe1/Å	N18(tz)-Fe1/Å	N5(tz)-Fe1/Å	tz FBF/°[g]	tz FBF/°[h]	tz FBF/°[i]	∑/°[j]	Fe1O1C31/°	Cl1-Fe1/Å	unit cell volume/Å^3
1	100	LS	1.9639(17)	1.9831(19)	1.955(2)	38.5(2)	21.8(2)	8.3(4)	25.2	—	5.3649(9)	2856.6(6)0
	300	LS	2.007(3)	2.022(4)	1.993(4)	36.0(5)	22.3(6)	9.9(10)	24.0	—	5.389(4)	2942(3)
2	100	LS	1.964(3)	1.993(3)[a]	1.963(4)[c]	8.1(6)	21.5(4)	39.5(4)	26.4	—	5.3834(12)	2884.9(4)
3	100	HS	2.1802(19)[a]	2.1635(19)[b]	2.1155(19)[e]	20.2(2)	36.4(2)	—	34.8	146.79(18)	6.0992(7)	3810.61(12)
4a	100	HS	2.206(2)[a]	2.182(2)[b]	2.098(3)[e]	23.0(3)	27.1(3)	—	25.0	136.3(6)	5.5589(7)	8220.1(4)
4b	100	HS	2.184(2)	2.178(2)	2.087(2)[e]	40.7(3)	38.3(3)	—	21.4	—	5.5069(10)	3637.2(3)
			2.186(2)[a]	2.176(2)[d]	2.110(3)[f]	27.0(3)	31.5(3)				5.3619(10)[k]	

[a] N6-Fe1. [b] N12-Fe1. [c] N17-Fe1. [d] N24-Fe1. [e] O1-Fe1. [f] O2-Fe1. [g] tz = N3N4N5N6C15 (N3N4N5N6C15 for **2**, **3**, **4a** and **4b**), FBF= F1B1F2 and tz = N15N16N17N18C45, FBF = F5B3F6 for **4b** second value, underlined atoms face toward the FBF plane. [h] tz = N9N10N11N12C30 (N9N10N11N12C30 for **4a**), FBF = F3B2F4 and tz = N21N22N23N24C60, FBF = F7B4F8 for **4b** second value, underlined atoms face toward the FBF plane. [i] tz = N15N16N17N18C45 (N15N16N17N18C45 for **2**), FBF = F5B3F6, underlined atoms face toward the FBF plane. [j] Sum of the deviation from 90° of all twelve *cis*-NFeN(O) angles. [k] Cl2-Fe1.

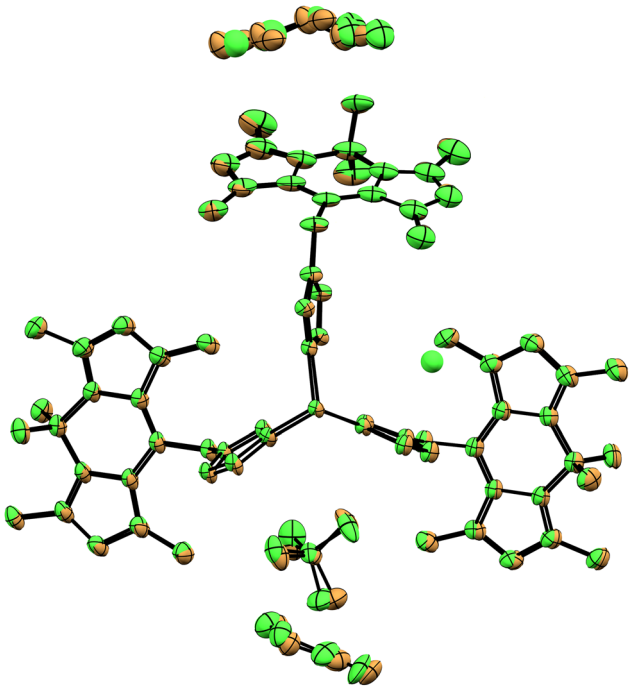

Fig. 2 Structure comparison of the asymmetric unit of coordination compound **1** (green) and **2** (gold) at 100 K, showing hardly any differences in the spatial arrangement of the ligands, non-coordinating anions and solvate molecules (ellipsoids: 50% probability level; H-atoms are omitted for clarity).

decreased octahedral ligand field splitting (Δ_o) due to the replacement of CH_3CN ligands with acetone. A weaker ligand field leads to the stabilization of the HS configuration.

Coordination compound **4a** crystallizes in the monoclinic *C*2/*c* space group and features one crystallographically unique mononuclear complex located on a twofold rotation axis (Fig. 4 and Fig. S14–S18). The heteroleptic complex adopts an octahedral geometry with four molecules of **L** coordinating *via* their tetrazolic *N*4-atom and two molecules of methanol functioning

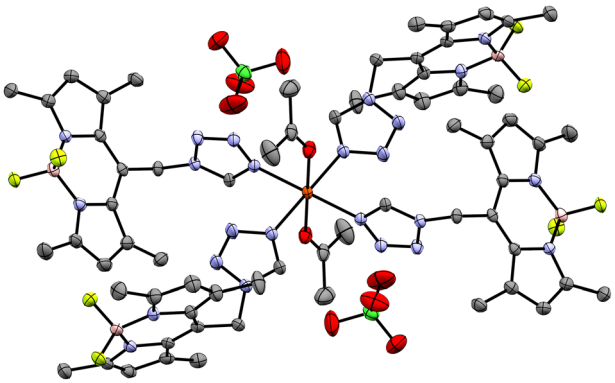

Fig. 3 Structure of coordination compound **3** at 100 K, featuring acetone as the co-ligand and ClO_4^- as the non-coordinating anion (ellipsoids: 50% probability level; atom color code: pink...B, grey...C, blue...N, light green...F, red...O, green...Cl, orange...Fe; H-atoms are omitted for clarity).

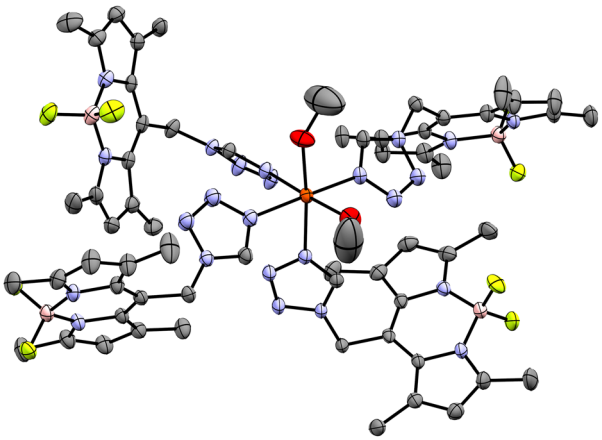

Fig. 4 Molecular structure of the heteroleptic mononuclear complex of coordination compound **4a** at 100 K, featuring methanol as the co-ligand in *cis* arrangement (ellipsoids: 50% probability level; atom color code: pink...B, grey...C, blue...N, light green...F, red...O, orange...Fe; non-coordinating anions, solvate molecules, minor positions of the disordered co-ligand and H-atoms are omitted for clarity).

as co-ligands. In contrast to **3** and earlier investigations,[32,33] where the co-ligands coordinate on the apical positions, in **4a** the co-ligand is coordinated by its O-atom in a *cis* arrangement. The C-atom (C31) of the methanol molecules is disordered about two positions with an occupancy ratio of 68.6 : 31.4(3). Based on the symmetry of **4a**, the complex features two pairs of crystallographically equivalent molecules of **L**; however, one pair of conformers is in *cis* arrangement and the other one in *trans* arrangement according to the twofold rotation symmetry. Like before, the different conformers exhibit different arrangements of the tz plane *vs.* the FBF plane.

Beside two non-coordinating anion molecules (ClO_4^-), for each mononuclear complex, there are two Et_2O molecules intercalated. We attribute remaining difference electron density to additional CH_3OH solvate molecules, which are realized when the C31-atom adopts its minor position. The O-atom of this molecule was modelled as disordered over four positions and the C-atom as disordered about the twofold axis.

SCs of **4a** stored under ambient conditions react with air humidity in a SC-to-SC topotactic transformation to form **4b**.[40]

4b crystallizes in the triclinic $P\bar{1}$ space group and features one crystallographically unique mononuclear complex located on a general position (Fig. S20). The complex of **4b** is built similar to **3**, but with water as co-ligand in the apical positions and all four molecules of **L** are crystallographically unique (Fig. S19). The inversion ($\bar{1}$) symmetry of the complex is disrupted by the ligands with the C-atoms C1 and C31. Thus, the structure can be considered as a modulated version of a hypothetic structure with halved *c*-axis. Again, for each mononuclear complex there are two non-coordinating anions intercalated; however, **4b** is devoid of any solvent molecules and shows no disorder (Fig. S21 and S22). The two coordinated water molecules form moderate-strength hydrogen bonds[41] with the ClO_4^- anions and the F-atoms of the **L** molecules in neighboring complexes. The donor–acceptor distances are listed in Table 2.

Table 2 Hydrogen bond parameters in **4b**

Donor atom (D)	H atom	Acceptor atom (A)	D–H/Å	H···A/Å	D···A/Å	D–H···A/°
O1	H1A	O10	0.86(3)	1.93(3)	2.776(3)	171(4)
O1	H1B	O7	0.87(3)	2.01(3)	2.826(5)	158(4)
O2	H2A	O4	0.86(3)	2.08(3)	2.895(4)	158(4)
O2	H2B	F1	0.86(3)	2.49(3)	3.228(3)	144(4)
O2	H2B	F2	0.86(3)	2.29(3)	2.845(3)	122(3)

The hydrogen bonds to the non-coordinating anions generate dimeric assemblies with two neighboring complexes along the [001] direction, whereas the hydrogen bonds to the F-atoms of the BODIPY moiety give rise to a one-dimensionally periodic hydrogen-bonding network extending along the [100] direction (Fig. 5 and Fig. S23-S25).

Similar to **3**, where acetone ligands favor the HS state, the coordination environments of **4a** and **4b** likewise stabilize the HS configuration, with N–Fe bond distances of the **L** molecules confirming HS character at 100 K.

XRPD measurements

The bulk powder X-ray diffraction pattern of **1** corresponds to the calculated reflections and the bulk can therefore be considered as single phase (Fig. S33). For **2**, the XRPD pattern predominately matches the calculated reflections of **2** (Fig. S34), but shows minor additional reflections, which may correspond to a heteroleptic $BrCH_2CN$ analogue of **3**, although the absence of suitable SCs prevented definitive identification.

The XRPD profile of **3** deviates from its simulated SC pattern, indicating incomplete phase purity or an unidentified secondary phase (Fig. S35). In contrast, the XRPD of **4** reveals an almost exclusive phase **4b** (Fig. S36), consistent with an immediate SC-to-SC transformation upon air exposure.

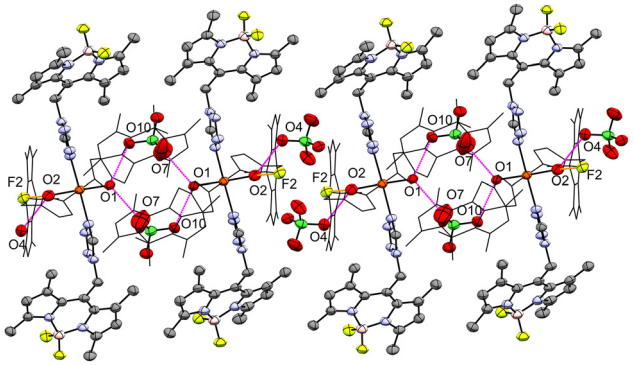

Fig. 5 H-bond network in **4b** at 100 K, forming dimers along the crystallographic *c*-axis (ClO_4^--bridges), with atomic number labeling of donor/acceptor O-atoms, and H-bonds represented as magenta-dotted lines (O–O) and orange-dotted lines (O–F) (ellipsoids: 50% probability level atom color code: grey...C, blue...N, light green...F, red...O, green...Cl, orange...Fe; H-atoms are omitted for clarity and **L** molecules are partly depicted as wireframes for better visualization).

IR spectroscopy

Upon coordination, the $\nu_{CH(tz)}$ band of **L** shifts from 3133 cm^{-1} to 3159 cm^{-1} in **1**, to 3160 cm^{-1} in **2**, to 3125 cm^{-1} in **3** and to 3144 cm^{-1} in **4b** (Fig. S37–S40). Comparable shifts were also observed in earlier investigations involving the same ligand.[32–34] The C=O stretching mode of the coordinated acetone molecules in **3** is evident at 1691 cm^{-1} as a sharp band. In **4b**, the broad O–H stretching band is visible at around 3370 cm^{-1}. As previously described,[32–34] the aliphatic C–H stretching vibrations (2990–2870 cm^{-1}) of **L** show no noteworthy change upon complexation. Furthermore, in the fingerprint region (1600–400 cm^{-1}), the only significant difference compared to the uncoordinated ligand in coordination compounds **1–4** is a band at 621 cm^{-1}, corresponding to the degenerate symmetric bending mode of the ClO_4^- anions.

Conclusions

In this work, we demonstrate that the steric demand of the ligand **L** can override the typical N4-coordination preference of monodentate 1*H*-tetrazoles in Fe(II) complexes. When XCH_2CN (X = Br, Cl) was employed as solvent, **L** occupied all four equatorial positions *via* its N4 donor, while also binding apically through its less basic N3 atom. This resulted in a pseudo-homoleptic $[Fe(\mathbf{L}^{N4})_4(\mathbf{L}^{N3})_2]^{2+}$ motif. To the best of our knowledge, this is the first example of monodentate 1*H*-tetrazole linkage isomerism in an Fe(II) complex. In contrast, steric crowding forced the formation of only heteroleptic $[Fe(\mathbf{L})_4(solvent)_2]^{2+}$ species *via* O-donor coordination when CH_3OH or $(CH_3)_2CO$ served as solvents. Furthermore, the CH_3OH derivative underwent an SC–SC topotactic transformation upon exposure to air moisture, exchanging CH_3OH for H_2O and forming a stabilized hydrogen bonding network in the $[Fe(\mathbf{L})_4(H_2O)_2](ClO_4)_2$ compound. Remarkably, the conversion from the *cis* to the *trans* arrangement did not cause crystal destruction.

Future work will focus on theoretical studies aimed at understanding why XCH_2CN yields a pseudo-homoleptic $[Fe(\mathbf{L}^{N4})_4(\mathbf{L}^{N3})_2]^{2+}$ complex, whereas other co-ligands (*e.g.* RCN,[33] $(CH_3)_2CO$, CH_3OH, H_2O) consistently give heteroleptic compounds. In parallel, we aim to define the precise steric threshold at which a N1-substituted tetrazole shifts from forming a homoleptic $[Fe(\mathbf{L})_6]^{2+}$ structure to a heteroleptic $[Fe(\mathbf{L})_4(solvent)_2]^{2+}$ motif. To this end, a series of N1-substituted tetrazoles with systematically varied substituent bulkiness is being synthesized. Comparing their Fe(II) coordination behavior, both experimentally and *via* DFT calculations, will reveal the critical substituent size that determines whether six 1*H*-tetrazole ligands can occupy all coordination sites, or if an O- or N-donor solvent must bind instead.

These insights will ultimately guide the rational design of 1*H*-tetrazole-based materials, whether for switchable magnetic applications, or advanced crystal engineering, in coordination chemistry and beyond.

Conflicts of interest

There are no conflicts to declare.

Data availability

The data supporting this article have been included as part of the Supplementary information (SI). Crystallographic data for **1**, **2**, **3**, **4a** and **4b** have been deposited at the CCDC under 2463767–2463772. Supplementary information: experimental protocols, crystal structure, XRPD spectra, and IR spectra. See DOI: https://doi.org/10.1039/d5nj03028e.

CCDC 2463767–2463772 contain the supplementary crystallographic data for this paper.[42a–f]

Acknowledgements

The authors thank Werner Artner (X-ray Center, TU Wien) for his assistance with XRPD measurements. For open access purposes, P. Weinberger has applied a CC BY public copyright license to any author accepted manuscript version arising from this submission.

Notes and references

1 V. A. Ostrovskii, E. A. Popova and R. E. Trifonov, in *Advances in Heterocyclic Chemistry*, ed E. F. V. Scriven and C. A. Ramsden, Academic Press, 2017, vol. 123, pp. 1–62.
2 F. R. Benson, *Chem. Rev.*, 1947, **41**, 1–61.
3 H. Zhao, Z. R. Qu, H. Y. Ye and R. G. Xiong, *Chem. Soc. Rev.*, 2008, **37**, 84–100.
4 Y. Yuan, M. Li, V. Apostolopoulos, J. Matsoukas, W. M. Wolf, M. A. T. Blaskovich, J. Bojarska and Z. M. Ziora, *Eur. J. Med. Chem.*, 2024, **279**, 116870.
5 M. Nasrollahzadeh, Z. Nezafat, N. S. S. Bidgoli and N. Shafiei, *Mol. Catal.*, 2021, **513**, 111788.
6 H. R. Meier and H. Heimgartner, *Tetrazole*, Georg Thieme Verlag, 8th edn, 1994.
7 P. N. Gaponik, S. V. Voitekhovich and O. A. Ivashkevich, *Russ. Chem. Rev.*, 2006, **75**, 569–603.
8 P. L. Franke, J. G. Haasnoot and A. P. Zuur, *Inorg. Chim. Acta*, 1982, **59**, 5–9.
9 G. Aromí, L. A. Barrios, O. Roubeau and P. Gamez, *Coord. Chem. Rev.*, 2011, **255**, 485–546.
10 R. M. Claramunt, D. Sanz, G. Boyer, J. Catalán, J. L. G. de Paz and J. Elguero, *Magn. Reson. Chem.*, 1993, **31**, 791–800.
11 W.-T. Liu, J.-Y. Li, Z.-P. Ni, X. Bao, Y.-C. Ou, J.-D. Leng, J.-L. Liu and M.-L. Tong, *Cryst. Growth Des.*, 2012, **12**, 1482–1488.
12 Z. Yan, M. Li, H. L. Gao, X. C. Huang and D. Li, *Chem. Commun.*, 2012, **48**, 3960–3962.
13 W. Zhang, F. Zhao, T. Liu, M. Yuan, Z. M. Wang and S. Gao, *Inorg. Chem.*, 2007, **46**, 2541–2555.
14 L. Sun, A. Rotaru, K. Robeyns and Y. Garcia, *Ind. Eng. Chem. Res.*, 2021, **60**, 8788–8798.
15 M. Quesada, H. Kooijman, P. Gamez, J. Sanchez Costa, P. J. van Koningsbruggen, P. Weinberger, M. Reissner, A. L. Spek, J. G. Haasnoot and J. Reedijk, *Dalton Trans.*, 2007, 5434–5440, DOI: 10.1039/b709460d.
16 A. Absmeier, M. Bartel, C. Carbonera, G. N. L. Jameson, F. Werner, M. Reissner, A. Caneschi, J. F. Létard and W. Linert, *Eur. J. Inorg. Chem.*, 2007, 3047–3054.
17 D. Müller, C. Knoll, B. Stoger, W. Artner, M. Reissner and P. Weinberger, *Eur. J. Inorg. Chem.*, 2013, 984–991.
18 M. Quesada, F. Prins, O. Roubeau, P. Gamez, S. J. Teat, P. J. van Koningsbruggen, J. G. Haasnoot and J. Reedijk, *Inorg. Chim. Acta*, 2007, **360**, 3787–3796.
19 G. N. L. Jameson, F. Werner, M. Bartel, A. Absmeier, M. Reissner, J. A. Kitchen, S. Brooker, A. Caneschi, C. Carbonera, J. F. Létard and W. Linert, *Eur. J. Inorg. Chem.*, 2009, 3948–3959.
20 C. M. Grunert, J. Schweifer, P. Weinberger, W. Linert, K. Mereiter, G. Hilscher, M. Muller, G. Wiesinger and P. J. van Koningsbruggen, *Inorg. Chem.*, 2004, **43**, 155–165.
21 M. Tafili-Kryeziu, M. Weil, T. Muranaka, A. Bousseksou, M. Hasegawa, A. Jun and W. Linert, *Dalton Trans.*, 2013, **42**, 15796–15804.
22 W. Zeni, M. Seifried, C. Knoll, J. M. Welch, G. Giester, B. Stöger, W. Artner, M. Reissner, D. Müller and P. Weinberger, *Dalton Trans.*, 2020, **49**, 17183–17193.
23 A. A. Soliman, M. M. Khattab, M. Reissner, P. Weinberger, F. Werner and W. Linert, *Inorg. Chim. Acta*, 2007, **360**, 3987–3996.
24 N. Hassan, P. Weinberger, K. Mereiter, F. Werner, G. Molnar, A. Bousseksou, M. Valtiner and W. Linert, *Inorg. Chim. Acta*, 2008, **361**, 1291–1297.
25 N. Hassan, J. Stelzl, P. Weinberger, G. Molnar, A. Bousseksou, F. Kubel, K. Mereiter, R. Boca and W. Linert, *Inorg. Chim. Acta*, 2013, **396**, 92–100.
26 D. Müller, C. Knoll, M. Seifried, J. M. Welch, G. Giester, M. Reissner and P. Weinberger, *Chem. – Eur. J.*, 2018, **24**, 5271–5280.
27 V. Braun, M. H. H. Wurzenberger, V. Weippert and J. Stierstorfer, *New J. Chem.*, 2021, **45**, 11042–11050.
28 V. Smeets, M. Wolff, J. A. Wolny, V. Schünemann, M. M. Dîrtu, J. Y. Ge, J. Vanacken, V. Moshchalkov and Y. Garcia, *Eur. J. Inorg. Chem.*, 2018, 394–413.
29 A. Tołoczko, M. Kazmierczak, M. Książek, M. Weselski, M. Siczek, J. Kusz and R. Bronisz, *Dalton Trans.*, 2024, **53**, 7163–7174.
30 A. Tołoczko, M. Kaźmierczak, M. Weselski, M. Siczek, M. Książek, J. Kusz and R. Bronisz, *Cryst. Growth Des.*, 2023, **23**, 1611–1621.
31 V. Maliuzhenko, M. Weselski, J. Gregolinski, M. Książek, J. Kusz and R. Bronisz, *Inorg. Chem.*, 2024, **63**, 17762–17773.
32 M. Huber, M. Schobinger, B. Stoger, M. Reissner and P. Weinberger, *Cryst. Growth Des.*, 2025, **25**, 8875–8885.
33 M. Huber, M. Schobinger, B. Stoger, M. Reissner and P. Weinberger, *Chem. – Eur. J.*, 2025, e01959, DOI: 10.1002/chem.202501959.
34 M. Huber, M. Schöbinger, J. Cirera, B. Stöger and P. Weinberger, *Eur. J. Org. Chem.*, 2025, e202401239.

35 M. Schöbinger, M. Huber, B. Stöger, C. Hametner and P. Weinberger, *CrystEngComm*, 2025, **27**, 2689–2697.
36 R. T. M. Fraser, *Linkage Isomerism*, American Chemical Society, 1967.
37 P. Gütlich, J. Jung and H. A. Goodwin, *Spin Transitions in Iron(II) Complexes*, Springer, Netherlands, Dordrecht, 1996.
38 A. Bialonska and R. Bronisz, *Inorg. Chem.*, 2010, **49**, 4534–4542.
39 A. Bialonska, R. Bronisz, M. F. Rudolf and M. Weselski, *Inorg. Chem.*, 2012, **51**, 237–245.
40 U. Müller and G. de la Flor, *Symmetry Relationships between Crystal Structures: Applications of Crystallographic Group Theory in Crystal Chemistry*, Oxford University Press, 1st edn, 2013, ch. 16, pp. 217–224.
41 T. Steiner, *Angew. Chem., Int. Ed.*, 2002, **41**, 49–76.
42 (*a*) CCDC 2463767: Experimental Crystal Structure Determination, 2026, DOI: 10.5517/ccdc.csd.cc2nprch; (*b*) CCDC 2463768: Experimental Crystal Structure Determination, 2026, DOI: 10.5517/ccdc.csd.cc2nprdj; (*c*) CCDC 2463769: Experimental Crystal Structure Determination, 2026, DOI: 10.5517/ccdc.csd.cc2nprfk; (*d*) CCDC 2463770: Experimental Crystal Structure Determination, 2026, DOI: 10.5517/ccdc.csd.cc2nprgl; (*e*) CCDC 2463771: Experimental Crystal Structure Determination, 2026, DOI: 10.5517/ccdc.csd.cc2nprhm; (*f*) CCDC 2463772: Experimental Crystal Structure Determination, 2026, DOI: 10.5517/ccdc.csd.cc2nprjn.